Mon. Not. R. Astron. Soc. **000**, 000–000 (0000) Printed 5 February 2008 (MN LATEX style file v1.4)

Spatial and Dynamical Properties of Voids in a ΛCDM Universe

Padilla, N.D.[1], Ceccarelli, L.[2], & Lambas, D.G.[2]

[1] *Departamento de Astronomía y Astrofísica, Pontificia Universidad Católica, V. Mackenna 4860, Santiago 22, Chile.*
[2] *IATE, Observatorio Astronómico de la Universidad Nacional de Córdoba, Laprida 851, 5000, Córdoba, Argentina.*

5 February 2008

ABSTRACT

We study statistical properties of voids in the distribution of mass, dark-matter haloes and galaxies ($B_J < -16$) in a ΛCDM numerical simulation populated with galaxies using a semi-analytic galaxy formation model(GALFORM, Cole et al. 2000). We find that the properties of voids selected from GALFORM galaxies are compatible with those of voids identified from a population of haloes with mass $M > 10^{11.5}\mathrm{h}^{-1}\mathrm{M}_{\odot}$, similar to the median halo mass, $M_{\mathrm{med}} = 10^{11.3}\mathrm{h}^{-1}\mathrm{M}_{\odot}$. We also find that the number density of galaxy- and halo-defined voids can be up to two orders of magnitude higher than mass-defined voids for large void radii, however, we observe that this difference is reduced to about half an order of magnitude when the positions are considered in redshift-space. As expected, there are outflow velocities which show their maximum at larger void-centric distances for larger voids. We find a linear relation for the maximum outflow velocity, $v_{\mathrm{max}} = v_0 r_{\mathrm{void}}$. The void-centric distance where this maximum occurs, follows a suitable power law fit of the form, $\log(d_{v\mathrm{max}}) = (r_{\mathrm{void}}/A)^B$. At sufficiently large distances, we find mild infall motions onto the sub-dense regions. The galaxy velocity field around galaxy-defined voids is consistent with the results of haloes with masses above the median, showing milder outflows than the mass around mass-defined voids. We find that a similar analysis in redshift space would make both outflows and infalls to appear with a lower amplitude. We also find that the velocity dispersion of galaxies and haloes is larger in the direction parallel to the void walls by $\simeq 10-20\%$. Given that voids are by definition sub-dense regions, the cross-correlation function between galaxy-defined voids and galaxies are close to $\xi = -1$ out to separations comparable to the void size, and at larger separations the correlation function level increases approaching the values of the auto-correlation function of galaxies. The cross-correlation amplitude of mass-defined voids vs. mass has a more gentle behaviour remaining negative at larger distances. The cross- to auto-correlation function ratio as a function of the distance normalised to the void radius, shows a small scatter around a relation that depends only on the object used to define the voids (galaxies or haloes for instance). The distortion pattern observed in $\xi(\sigma,\pi)$ is that of an elongation along the line of sight which extends out to large separations. Positive ξ contours evidence finger-of-god motions at the void walls. Elongations along the line of sight are roughly comparable between galaxy-, halo- and mass-defined voids.

Key words: large-scale structure of Universe, methods: N-body simulations, galaxies: kinematics and dynamics cosmology: theory

1 INTRODUCTION

Voids can be thought of as large volumes with very low galaxy density surrounded by the walls and filaments of the cosmic web. These objects were first detected by Gregory & Thompson (1978), Joeever, Einasto & Tago (1978), Kirshner et al. (1981) and Geller & Huchra (1989). Soon after their discovery, White (1979), Hoffman & Shaham (1982) and Peebles (1982) derived theoretical statistical properties of voids and related them to the gravitational instability scenario. Einasto, Einasto & Gramann (1989) also estimated sizes of voids in different samples of galaxies in redshift surveys and compared their results with numerical simulations.

The characteristics of voids in the galaxy distribution, such as the void probability distribution were studied by Vogeley et al. (1994), Ghigna et al. (1996), and Müller et al. (2000), whereas the fraction of the total volume in the Universe occupied by voids, which was found to add up to about 50%, was measured by El-Ad & Piran (1997, 2000), Plionis & Basilakos (2002), and Hoyle & Vogeley (2002). Peebles (2001) presents a detailed review of the observational works devoted to void statistics.

More recently, theoretical studies on the characteristics of voids and their surrounding structure have concentrated on several different aspects. For instance, van de Weygaert (2004) presented an excursion set approach (Bond et al. 1991) for predicting the distribution function of void sizes and its evolution with redshift. Patiri et al. (2004) also carry out an excursion set study on voids, and are able to characterize the number density of voids as a function of void radius as well as the mass function of haloes in voids. Their model takes into account the fact that the properties of voids depend on the haloes used to identify them (Gottlöber et al., 2003, and references therein). Based on this result, Patiri et al. provide a framework which allows a comparison between theoretical predictions and statistical measures of voids found in the distribution of the visible galaxies that populate haloes. Also, taking into account the nearly spherical average shape of voids, Ryden (1995) showed that it is possible to use the cosmologically induced redshift-space distortion in the apparent shape of intermediate redshift voids to measure the deceleration parameter, q_0.

On the observational side, only very recently it has become possible to perform accurate statistical studies of voids using real data. For instance, Croton et al. (2004) used the 2-degree Field Galaxy Redshift Survey (2dFGRS) to measure the reduced void probability function (RVPF), which connects the distribution of voids to the higher moments of galaxy counts in cells. These new redshift surveys also allow the study of the population of galaxies inside voids. Hoyle et al. (2003) use the Sloan Digitized Sky Survey (SDSS) to study the luminosity function of void galaxies, which they find by setting an upper limit on the local density contrast at the galaxy position, $\delta\rho/\rho \leq -0.6$. They find that galaxies are fainter in voids, but that the faint-end slope of the luminosity function, is consistent with that of galaxies in higher density environments. Also using the SDSS, Goldberg et al. (2004) study the mass function of void galaxies selected using the same density threshold as Hoyle et al. (2003), finding that galaxies in voids are nearly unbiased with respect to the mass.

In this paper we carry out a comprehensive numerical study of the dynamical and spatial properties of galaxies, dark-matter particles and haloes with respect to void centres. We study how the properties of voids identified from the distribution of dark-matter particles and haloes in a simulation relate to those of voids identified from the galaxy distribution. Goldberg et al. find that galaxies trace the distribution of mass within voids, a fact that contrasts with the large biases expected in higher density environments, such as walls, filaments and clusters. Since these objects set the boundaries of voids, this study provides a useful insight on the global segregation pattern of dark-matter and galaxies. The study of the effects of observational biases occurring in flux limited redshift surveys, and an application of the statistics presented here to observational catalogues are carried out in a forthcoming paper, Ceccarelli et al. (2004a).

This paper is organised as follows. Section 2 describes the semi-analytical numerical simulation used in this work and the procedure adopted for identifying voids in the simulation box. Section 3 analyses the outflow signatures that characterise the regions surrounding voids. In section 4 we study the spatial 2-point cross-correlation functions between voids and different tracers, dark-matter particles, haloes and galaxies. Finally, section 5 summarises our results and presents the main conclusions extracted from this work.

2 VOIDS IN THE NUMERICAL SIMULATION

In this work we study void statistics using a ΛCDM numerical simulation which contains 125 million dark matter particles and ~ 2 million galaxies from the GALFORM semi-analytic galaxy formation model (Cole et al. 2000), kindly provided by the Durham group. There are approximately $650,000$ dark-matter haloes with at least 10 members, identified from the distribution of datk-matter particles in the simulation using a Friends-of-Friends (FOF from now on) algorithm with a linking length $b_{\rm FOF} = 0.2$. The resulting haloes are characterised by a minimum mass of $M_{\rm min} = 1.05\ 10^{11}{\rm h}^{-1}{\rm M}_{\odot}$, a median mass $M_{\rm med} = 2\ 10^{11}{\rm h}^{-1}{\rm M}_{\odot}$, and a maximum $M_{\rm max} = 2\ 10^{15}{\rm h}^{-1}{\rm M}_{\odot}$. It should be noticed that the FOF algorithm does not resolve substructure within the dark-matter haloes. The semi-analytic model output consists of approximately 2 million galaxies with $B_J < -16$ at $z = 0$ (from now on, we will refer to all galaxies above this magnitude limit, simply as galaxies) in the simulation. The 25, 50 and 75 percentiles of the haloes hosting at least one galaxy are $1.57\ 10^{11}{\rm h}^{-1}{\rm M}_{\odot}$, $3.17\ 10^{11}{\rm h}^{-1}{\rm M}_{\odot}$, and $8.95\ 10^{11}{\rm h}^{-1}{\rm M}_{\odot}$ respectively. We now describe the simulation parameters: the box side measures $250{\rm h}^{-1}$Mpc, the matter density parameter corresponds to $\Omega_m = 0.3$, the value of the vacuum density parameter is $\Omega_\Lambda = 0.7$, the Hubble constant, $H = h100{\rm kms}^{-1}{\rm Mpc}^{-1}$, with $h = 0.7$, and the primordial power spectrum slope is $n_s = 0.97$. The present day amplitude of fluctuations in spheres of $8{\rm h}^{-1}$Mpc is set to $\sigma_8 = 0.8$. This particular cosmology is in line with recent cosmic microwave background anisotropy (WMAP, Spergel et al. 2003) and large scale structure (2dFGRS, Percival et al. 2004) measurements.

We use this simulation to study the dynamical and spatial characteristics of galaxies, dark-matter haloes and dark-matter particles around voids. Throughout this paper, errors in the statistics are calculated using the jackknife method, which has been shown to provide equivalent errors to those found by applying the statistics to a large number of independent simulations and measuring a variance (see for instance, Croton et al. 2004, Padilla & Baugh, 2003). These results indicate that jackknife errors provide a reasonable estimate of statistical uncertainties and cosmic variance.

The use of semi-analytic numerical simulations allows a comparison of galaxy-, halo- and mass-defined voids, since the population of galaxies in the simulation box is physically motivated, subject to evolution via mergers, metal enrichment, dust evolution, and other important astrophysical processes (for full details see Cole et al. 2000).

Throughout this paper we compare results from real-

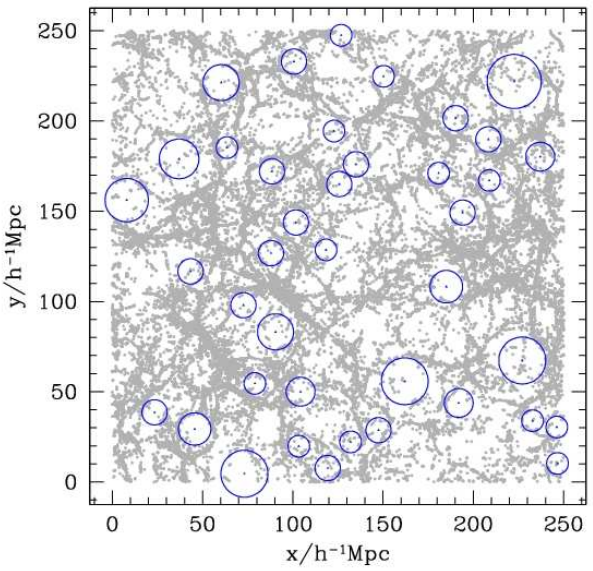

Figure 1. Slice of the numerical simulation box, corresponding to $100 < z/\mathrm{h}^{-1}\mathrm{Mpc} < 110$, showing the positions of semi-analytic galaxies (black dots) and voids found from the galaxy positions (gray dots). The circles indicate the spatial extent of the voids.

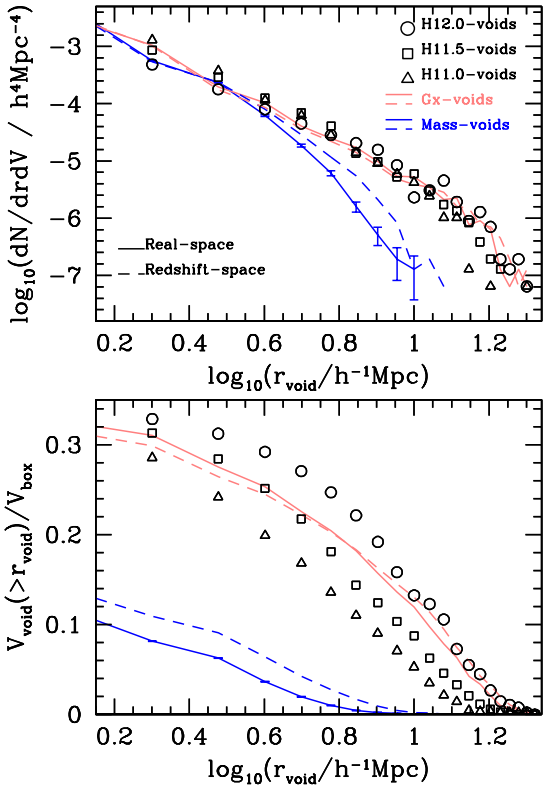

Figure 2. Upper panel: Number density of voids as a function of void size. The blue (black) lines correspond to voids found from the distribution of dark-matter in the simulation box. Red (gray) lines show the results obtained from the simulation galaxies. The symbols represent results from the distribution of H11-, H11.5- and H12-defined voids (triangles, squares and circles respectively). The solid and dashed lines correspond to the number density of voids found from positions of objects in real- and redshift-space respectively. Lower Panel: cumulative volume fraction in voids of radius $r > r_{\rm void}$. Lines, colours and symbols are as in the upper panel.

and redshift-space derived quantities. When referring to voids this indicates that, when identifying voids in the simulation, the positions of particles, haloes or galaxies were considered either in real- or redshift-space. We implement redshift-space positioning in this simulation by displacing the $z-$coordinates of particles and galaxies by the $z-$component of their velocities in units of h^{-1}Mpc (distant observer looking down the $z-$axis).

In the next subsections we describe the void finding algorithm, present the resulting number density of voids as a function of void radius, and calculate the void auto-correlation function.

2.1 Void finding algorithm

We find voids in the simulation by identifying spherical volumes where the overall density contrast satisfies $\delta = -0.9$, which corresponds to a usual definition of an under-dense region. Later in this section we find that small variations on this condition do not affect significantly our statistics. We use the mass, dark-matter haloes, and the galaxies in the simulation to find voids, and we also investigate in a simple way the effects of redshift space distortions in the identification of voids. Therefore, we produce ten different catalogues of voids in the numerical simulation. We first have 5 sets of voids, found in the distribution of dark-matter (which we will refer to as mass-defined voids), haloes with masses above 10^{11}, $10^{11.5}$ and $10^{12}\mathrm{h}^{-1}\mathrm{M}_{\odot}$ (halo-defined voids, also referred to as H11-, H11.5- and H12-defined voids respectively)*, and voids found in the distribution of galaxies (referred to as galaxy-defined voids) in real space. Repeating the identification in redshift-space provides us with the remaining 5 samples.

For each of these different samples of voids, the procedure followed is exactly the same, and comprises the following steps:

- We produce a large number of random positions which will be used to test whether the density contrast in spheres centred on these positions satisfies the condition $\delta < -0.9$. The higher the number of random positions the higher the accuracy in finding the true centre of a void in the simulation.
- We calculate the density contrast as a function of radius of a sphere centred on the random positions generated in the first step.
- We identify the radii for which the void density criterion $\delta < -0.9$ is satisfied. In the event where this condition is satisfied more than once at different radii, we only consider the largest radius.
- Up to this point, the outcome of the identification process will likely consist of a large number of underdense over-

* The halo mass thresholds are selected so as to have samples of haloes with space densities differing by half an order of magnitude; H11 haloes characterised by $n = 5\ 10^{-3}$, H11.5 by $n = 1.5\ 10^{-3}$, and H12 haloes by $n = 5\ 10^{-4}$

laping spheres. Therefore, the last step consists of removing all spheres overlapping with a larger void. For instance, this last step will make a large underdense spherical region of radius r be represented by a single sphere of radius r, instead of by many spheres of smaller radius that could be able to fill the underdense volume.

The nature of the finding algorithm makes voids of comparable sizes at similar positions be simply replaced by a larger void which naturally occupies the volume of all the smaller voids together.

We have made several checks to make sure the void finding algorithm is reliable. We have varied the upper limit in δ up to $\delta < -0.6$, and find that in general results are not significantly affected in the case of galaxy- and halo-defined voids. The main difference resides in the appearance of large spurious ($r_{\rm void} > 30{\rm h}^{-1}$Mpc) voids.

We have also checked that the removal of overlapping voids does not affect significantly the mean values of the statistics we investigate in this work by allowing for instance, voids within voids. It is important, however, to take this effect into account when calculating errors, since many slightly de-centred voids representing only one physical void in the simulation artificially lowers the size of statistical errors.

Given that dark-matter particles outnumber galaxies by a factor $\simeq 100$ in the simulation, we tested for the impact of the number of particles in the identification procedure. In order to do this we select 1/100th of the total dark-matter particles and run our void identification algorithm. The resulting void catalogue is almost identical to the one found from the full simulation.

Figure 1 shows a slice of the simulation box with the distribution of semi-analytic galaxies and the positions of voids found by our procedure. In order to improve clarity, in this particular plot we only show voids with radii in the range $10 < r_{\rm void}/{\rm h}^{-1}$Mpc. As can be seen, the void identification algorithm is quite satisfactory, picking out low density regions with void radii compatible with the observed galaxy distribution. The empty spaces not filled with voids are expected for instance from voids with $r_{\rm void} < 10{\rm h}^{-1}$Mpc, or voids with centres outside the slice shown in this figure.

2.2 Void number density

The first statistic we measure using the voids identified in the previous subsection is the number density as a function of void radius, $r_{\rm void}$. We show the measured results from the simulation box in the upper panel of figure 2, where the red (gray) lines correspond to voids found from the spatial distribution of galaxies and the blue (black) lines from the mass. Solid lines correspond to real-space, dashed lines to redshift-space. Symbols show the results from the distribution of voids identified from haloes of different masses as indicated in the key. It is noticeable the good agreement between these estimates for $r < 4{\rm h}^{-1}$Mpc, where all the void number densities are virtually indistinguishable. At larger object/void-centre separations the different estimates start to diverge. For instance the difference between real- and redshift-space estimates can diverge by as much as a factor of $\simeq 2.5$, as is the case at large mass-void radii $r_{\rm void} > 10{\rm h}^{-1}$Mpc. This is attributable to the fingers of god effect which takes place in the void walls and displaces dark-matter particles from the walls and dilutes the void boundaries. Galaxy- and halo-void number densities are not significantly affected by a redshift-space identification of voids as expected, since the peculiar velocities of mass and galaxies are small ($v/H_0\ 1h^{-1}Mpc$) compared to the void sizes. The difference between number densities of voids found from the distribution of galaxies and mass starts to be noticeable at separations $> 4{\rm h}^{-1}$Mpc; eventually there are no longer mass-defined voids with $r_{\rm void} > 10{\rm h}^{-1}$Mpc whereas it is still possible to identify galaxy-defined voids with $r_{\rm void} > 20{\rm h}^{-1}$Mpc. The number density of halo-defined voids is more comparable to that of galaxy-defined voids.

The increase in the number density of voids with the mass of the haloes used to identify them can be understood in terms of the bias factor between haloes and the mass. Higher mass haloes are more strongly biased with respect to the mass, and therefore are preferably found in high mass density regions, which correspond preferably to the centres of void walls and filaments. The net effect this would have is to increase the radius of the void when identified from a biased population of objects, and would explain the apparent increase in number density observed in figure 2.

From the number density of voids, it is straight-forward to obtain the fraction of volume inside voids in the simulation. The lower panel of fig. 2, shows the volume inside voids with $r > r_{\rm void}$. As can be seen, the difference between mass- and galaxy-defined voids is even more evident here. Also, it is now possible to recognise a good agreement between galaxy-defined voids and H11.5- for $r_{void} < 6{\rm h}^{-1}$Mpc and H12-defined with $r_{void} > 6{\rm h}^{-1}$Mpc voids.

This demonstrates that caution should be taken when analysing properties of galaxy-defined voids, which can differ from those of halo- and mass-defined voids. As mentioned above, the reason for this discrepancy is the slightly biased nature of the galaxy distribution in this simulation with respect to the dark-matter particles and haloes. In particular, the spatial distribution of galaxies shows larger and more numerous voids than the distributions of mass or low mass haloes (less biased populations). Given that the redshift-space effect enhances the number density of mass-defined voids more strongly, the differences between results from mass- and galaxy-defined voids are less important in redshift-space.

The volume fraction inside voids can be as large as 30%, a value which is slightly lower than estimates from redshift surveys of 50% by El-Ad & Piran, 1997, 2000, Plionis & Basilakos, 2002, and Hoyle & Vogeley, 2002. As pointed out above, our estimate of the volume fraction is only an order of magnitude estimate at best, since our simulated volume is limited and we might be badly affected by sampling statistics in the large-volume end of the void population.

2.3 Void 2-point auto-correlation function

A simple statistics that can be applied to the void positions is the 2-point auto-correlation function. The advantages in studying the correlation function relies in its widespread use and in its direct connection to the power spectrum of density fluctuations.

The upper panel of figure 3 shows the auto-correlation function of galaxy- (symbols) and H12- and H11.5-defined voids (dashed, $M > 10^{12}{\rm h}^{-1}{\rm M}_{\odot}$, solid, $M > 10^{11.5}{\rm h}^{-1}{\rm M}_{\odot}$)

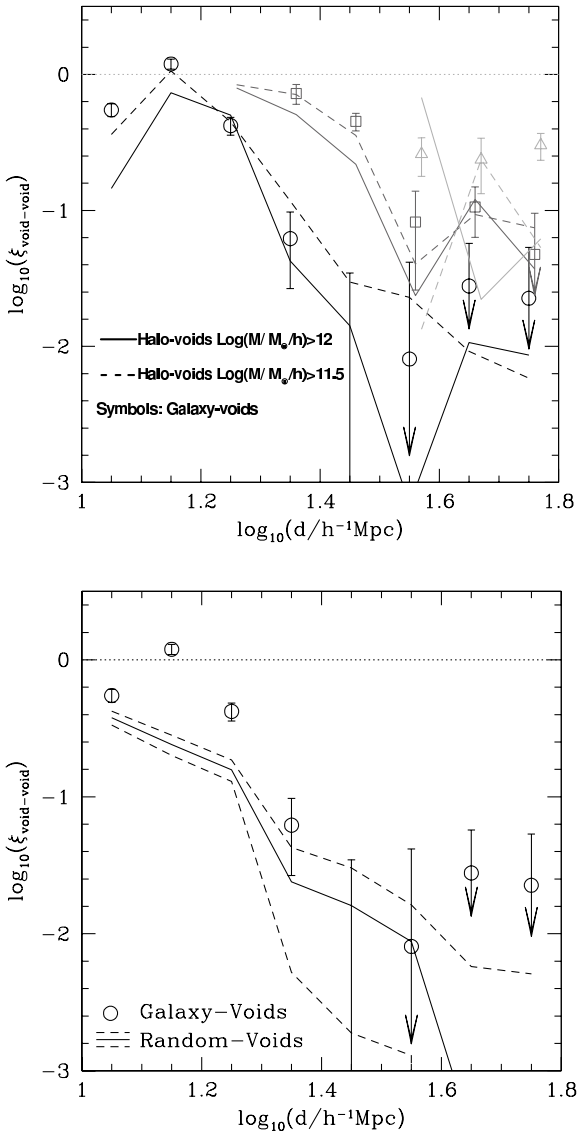

Figure 3. Top panel: void 2-point auto-correlation function for voids with radii in the ranges $4 < r_{\rm void}/h^{-1}Mpc < 8$ (Black lines and circles), $8 < r_{\rm void}/h^{-1}Mpc < 12$ (dark-grey lines and squares), and $16 < r_{\rm void}/h^{-1}Mpc < 20$ (light-grey lines and triangles). The symbols represent results from galaxy-defined voids, the lines from halo-defined voids. Bottom panel: comparison between the auto-correlation function of galaxy- and random-voids with the same number density as a function of void radius.

for different void radii (gray scale and different symbols as indicated in the figure caption) †. As can be seen, larger voids are more strongly clustered, and show a positive correlation signal out to larger separations. The amplitude of these correlations, however, is quite low and we only find a significant signal out to scales $\simeq 50{\rm h}^{-1}$Mpc. It is interesting to note that at scales larger than $15{\rm h}^{-1}$Mpc, the slopes of the correlation functions for voids of different radii are similar. The auto-correlation function of voids defined using the most massive haloes (H12, dashed lines) provides the best match to the clustering of galaxy-defined voids.

In order to assess whether the correlation function responds to an effect of the void identification procedure, we show in the lower panel of figure 3 the average correlation function (and $1-\sigma$ confidence region) of 100 sets of randomly placed spheres (random-voids). Each of these sets has the same number density as a function of radius than galaxy-defined voids, and also follows the exclusion constraints set for the identification of galaxy-defined voids. Also, random-voids are placed in a volume with the same size as the simulation box. As can be seen, the exclusion constraint alone can produce a non-zero correlation function consistent with a power law of index $\simeq -3$. The comparison with the galaxy-defined voids correlation function, however, shows that the amplitude of the galaxy-void correlation function is still significantly higher than that of the random-voids. This could be interpreted as evidence of the influence of hierarchical clustering in the spatial distribution of galaxy-defined voids.

We also calculated the correlation function of sets of random-voids with a different number density as a function of void radius, in particular, similar to that of H11-defined voids. We find that the comparison between H11-defined voids and this new set of random-voids is identical to the comparison we carry out above, namely that the correlation function of H11-defined voids is higher in amplitude than that of random-voids for small separations.

Our preliminary conclusion from the study of the number density of voids and void auto-correlation functions in the numerical simulation is that galaxy-defined voids show good agreement with voids identified from moderate to high mass haloes ($M > 10^{11.5}{\rm h}^{-1}{\rm M}_\odot$). From now on, we will mostly compare results from these two sets of voids, unless we state otherwise.

3 THE PECULIAR VELOCITY FIELD AROUND VOIDS

Just as it has recently become possible to study the peculiar velocity field around groups (Ceccarelli et al. 2004b, C05 from now on), which is characterised by infall galaxy motions toward the group centres, it is also possible to study outflows of material escaping the void volumes. A further motivation to study the outflow motions is that as has been shown by C05, the infall motions of mass and galaxies are almost identical, being the galaxy infalls only slightly higher than the mass infalls. It may be possible then, to obtain a reliable measurement of the bulk outflows of mass emptying the void volumes by studying the velocities of galaxies around voids.

We set out to compare the outflows of mass, dark-matter haloes, and galaxies from the simulated void catalogues constructed in this work. In order to do this we simply project the peculiar velocity of galaxies and dark-matter haloes and particles onto the radial direction measured towards the void centres. Adding the contribution from all the individual particles, haloes or galaxies together, and av-

† The number of centres used in the computation of the void-autocorrelation function is roughly 3000, 280, and 15, for the three ranges of void radii shown in figure 3 (smaller to larger void radii, respectively), which explains the noise present in the correlation functions of voids of large radius.

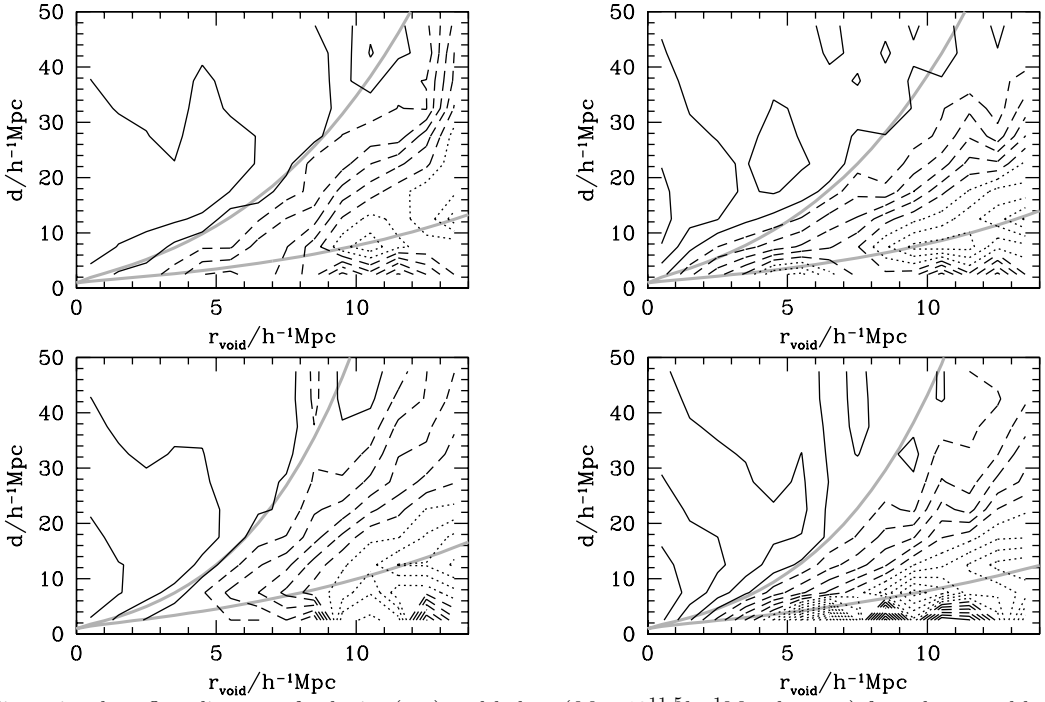

Figure 4. 2-dimensional outflow diagram of galaxies (top) and haloes ($M > 10^{11.5}\mathrm{h}^{-1}\mathrm{M}_{\odot}$, bottom) for galaxy- and halo-defined voids identified from real- and redshift-space data (left and right respectively). The x-axis corresponds to voidsize, the y-axis to distance from the void centre. Solid lines show inflow velocities $v_{\rm out}/\mathrm{kms}^{-1} = 0, 20, 40, ...$ (positive velocities), dashed lines show outflow motions, $v_{\rm out}/\mathrm{kms}^{-1} = -20, -40, -60, -80$ and -100 (negative velocities), and dotted lines show stronger outflows, $v_{\rm out}/\mathrm{kms}^{-1} = -120, -140$, and so forth. The thick gray solid lines show fits from eq. 1 for $d_{\rm vmin}$ and $d_{\rm zero}$ (lower and upper lines respectively). The best fit parameters are shown in table 1.

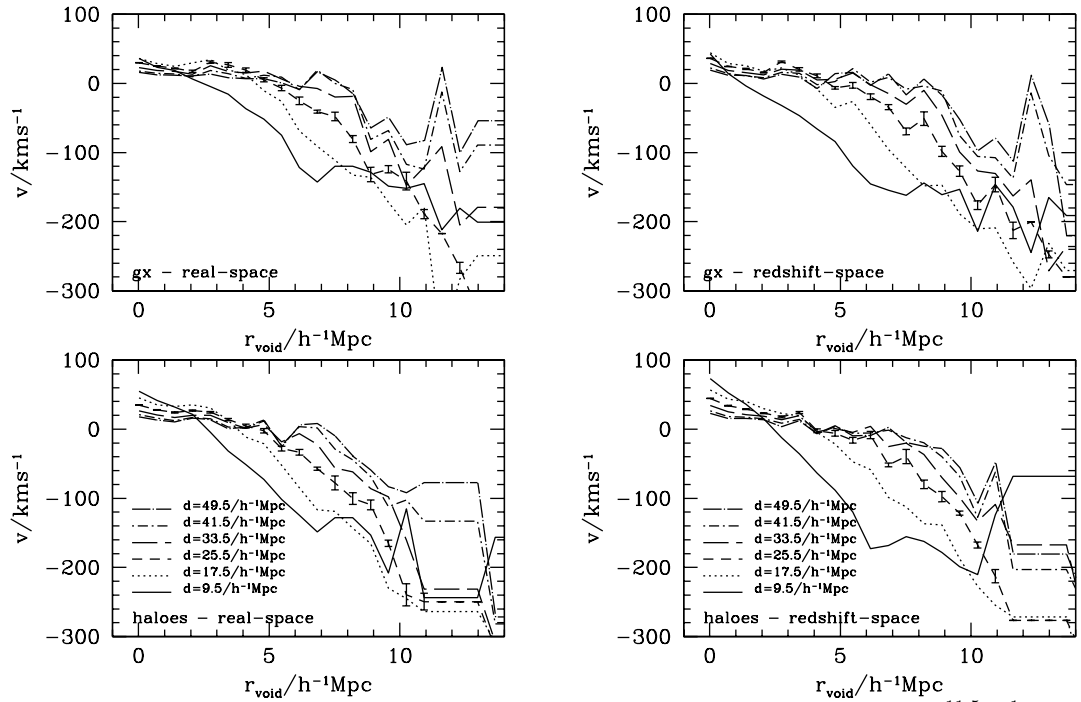

Figure 5. Outflow velocities as a function of void radius, $r_{\rm void}$, of galaxies (top) and haloes ($M > 10^{11.5}\mathrm{h}^{-1}\mathrm{M}_{\odot}$, bottom) around galaxy- and halo-defined voids respectively, identified from real- and redshift-space data (left and right panels respectively). In order to improve clarity, jackknife errorbars are only shown for $d = 25.5\mathrm{h}^{-1}\mathrm{Mpc}$. Ranges in d are shown in the key.

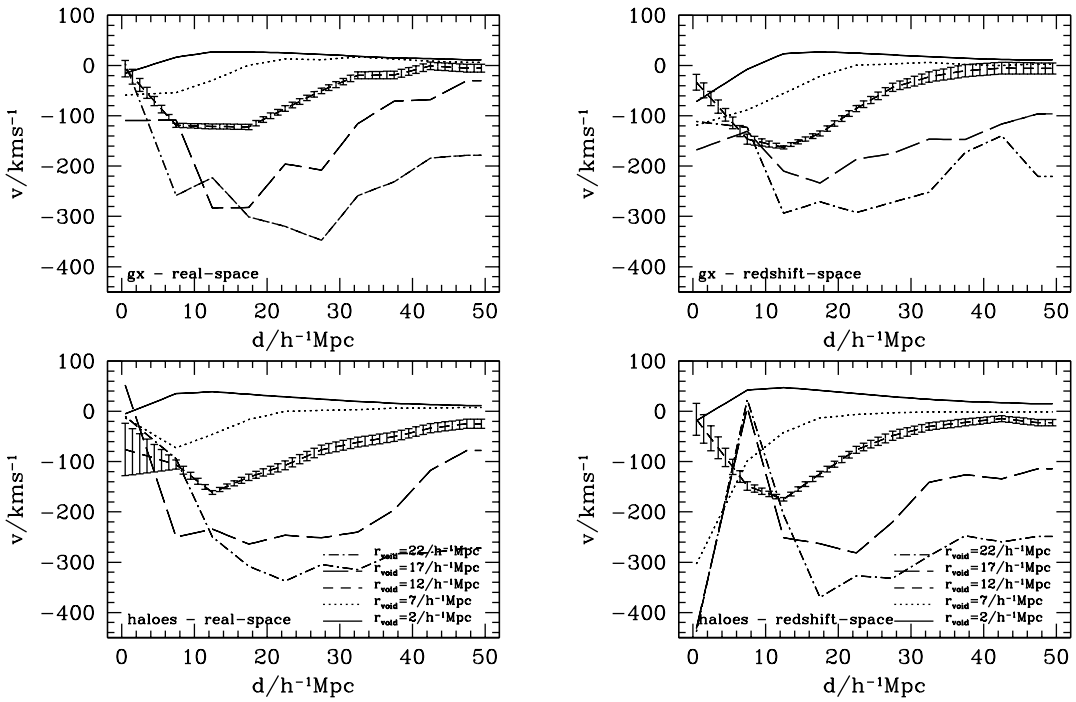

Figure 6. Outflow velocities as a function of distance from the void centre for galaxies (top) and haloes (bottom), around galaxy- and halo-defined voids identified from real- and redshift-space data (left and right panels respectively). In order to improve clarity, jackknife errorbars are shown only for $r_{\rm void} = 12{\rm h}^{-1}{\rm Mpc}$. Ranges in $r_{\rm void}$ are shown in the key.

eraging the result, we obtain a dependence of the outflow motions as a function of distance to the void, d, and void radius, $r_{\rm void}$. Defined in this way, a positive velocity indicates an infall to-wards the void centre, and a negative velocity, an outflow.

Figure 4 shows the 2-dimensional diagrams of outflow velocities as a function of void size (x-axis) and distance (y-axis). The lines show constant outflow velocity levels; solid lines correspond to positive velocities (infalls), and dashed and dotted lines show negative velocities or outflows (see the figure caption for velocity level values). Lower panels in this figure show results for halo velocities around H11.5-defined voids. Upper panels show results for galaxy velocities around galaxy-defined voids. As can be seen from the comparison of the iso-velocity contours in the upper and lower panels, the velocities around halo-defined voids reach higher values of both, infall and outflow motions, than around galaxy-defined voids by approximately $20{\rm kms}^{-1}$ (see also figure 6). However, if we concentrate on the velocity minimum for large $r_{\rm void}$ voids, we see that there is an agreement between results from haloes and galaxy-defined voids. Also, small voids, $r_{\rm void} \leq 7{\rm h}^{-1}{\rm Mpc}$, show infall motions at separations $d(r_{\rm void}) \geq 20{\rm h}^{-1}{\rm Mpc}$. This indicates the existence of overdense regions surrounding small voids, which would be responsible for producing the observed infall motions.

We provide a fit for the distance at which the outflow motions reach $v = 0{\rm kms}^{-1}$,

$$\log(d_{\rm zero}^{mass,r}) = \left(\frac{r_{\rm void}}{A}\right)^B. \quad (1)$$

In the case of H11.5 velocities and H11.5-defined voids we find $A = 3.0{\rm h}^{-1}{\rm Mpc}$ and $B = 0.6$, and for galaxy-defined voids and galaxies, $A = 3.5{\rm h}^{-1}{\rm Mpc}$ and $B = 0.7$. (for values of the parameters A and B for the other simulated samples, and in redshift-space, see table 1). At larger distances from the void centre, velocities become positive, indicating an opposite infall motion.

The distance from the void centre where the minimum in outflow velocity occurs, $d_{\rm vmin}$, is very well approximated by

$$d_{\rm vmin} = r_{\rm void}. \quad (2)$$

Motivated by the results for $d_{\rm zero}$, we can also fit eq. 1 to $d_{\rm vmin}$. This equation could prove to be more accurate for larger voids. In the case of H11.5 velocities in real-space, the best fit parameters are $A = 2.5{\rm h}^{-1}{\rm Mpc}$ and $B = 0.6$. For galaxy-defined voids and galaxies, $A = 3.6{\rm h}^{-1}{\rm Mpc}$ and $B = 0.7$. The best fit parameters for all the samples studied here can be found in table 1.

The fits corresponding to $d_{\rm vmin}$ and $d_{\rm zero}$ as a function of the void radius are shown in all panels of figure 4 in thick solid gray lines (lower and upper lines respectively).

The fit parameters corresponding to different halo masses correlate reasonably well with halo mass, and can therefore be used to interpolate for samples of masses different than the ones used in this paper. Alternatively, this can also be used when analysing a sample of galaxies for which the masses of haloes in which they reside are known. This is also applicable to other fits provided in this work (Equations 3 and 5).

We now focus on the dependence of the outflow velocities on void radius at fixed distances from the void centres. We show this dependence in figure 5 where the left panels show results in real-space and right panels in redshift-space.

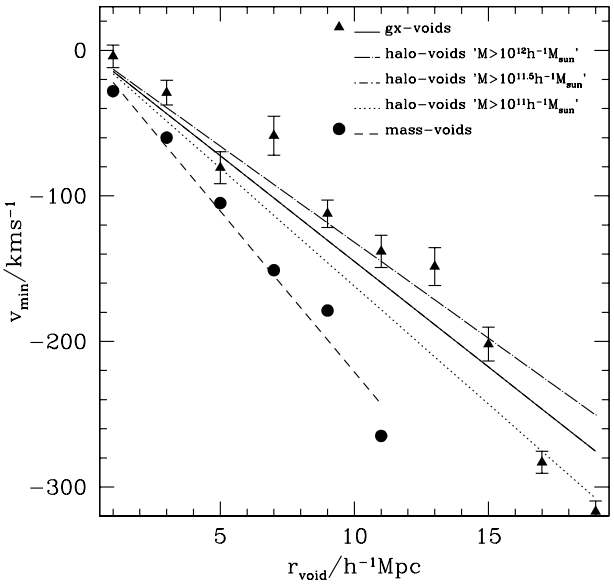

Figure 7. Maximum outflow velocity as a function of void radius for galaxies (triangles) and dark-matter particles (blue/black circles), around galaxy- and mass-defined voids identified from real-space data. The lines show the linear fits to the points, $v_{\rm min} = v_0 r_{\rm void}$ (dashed and solid lines). Dotted, dot-dashed, and long-dashed lines correspond to linear fits to the minimum velocity found for H11-, H11.5-, H12-defined voids. Errorbars show the 1-σ confidence errors calculated using the jackknife method.

Table 1. Best fit parameters, A and B, for the relation between void radius and the distance at which the maximum outflow is measured ($d_{\rm vmin}(r_{\rm void})$), and for the distance at which $v = 0$ ($d_{\rm zero}(r_{\rm void})$). We present the best fit parameters for voids selected from the distribution of mass and galaxies, and in real- and redshift-space.

Statistic	Real/Redshift-space	Gx./mass	AhMpc^{-1}	B
$d_{\rm vmin}$	Real	Mass	2.30	0.80
		H11	2.50	0.60
		H11.5	2.50	0.60
		H12	2.50	0.60
		Gx.	3.60	0.70
	Redshift	Mass	3.00	0.80
		H11	2.80	0.60
		H11.5	3.00	0.60
		H12	3.00	0.50
		Gx.	3.50	0.70
$d_{\rm zero}$	Real	Mass	0.10	0.38
		H11	1.00	0.65
		H11.5	1.20	0.65
		H12	1.70	0.65
		Gx.	1.00	0.55
	Redshift	Mass	0.10	0.37
		H11	1.00	0.65
		H11.5	1.30	0.65
		H12	1.70	0.65
		Gx.	0.95	0.55

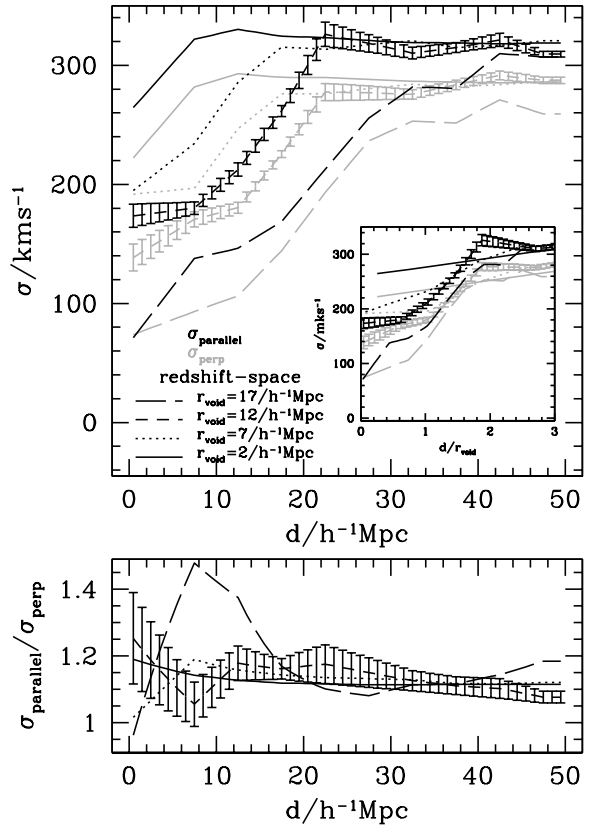

Figure 8. Upper panel: Velocity dispersions in the directions parallel (black lines) and perpendicular (gray lines) to the void walls for galaxy-defined voids, as a function of distance to the void centre. Different line types correspond to different void radii. Error-bars are only shown for the $r_{void} = 12{\rm h}^{-1}$Mpc for clarity, and are calculated using the Jacknife method. The inset shows the velocity dispersions as a function of normalised distance to the void centre. Lower panel: ratio between velocity dispersions parallel and perpendicular to the void walls. Line types are as in the upper panel.

Upper panels correspond to galaxies and galaxy-defined voids, and lower panels to H11.5 haloes and H11.5-defined voids. The different line types show the outflow velocities at different distances from the void centres (the key in the figure specifies their values). The outflow velocities at different distances show a complicated variation as we go from regions near the void centres to large distances. For instance, it is easy to find mild infall motions $v < 50{\rm kms}^{-1}$ near the centres of moderate sized voids with $r_{\rm void} < 5{\rm h}^{-1}$Mpc. Also, the smaller the distance to the void centre, the smaller the void at which an outflow motion (negative velocities) can be found. The trend of velocities around voids with increasing void radius is negative for $r_{\rm void} \geq 5{\rm h}^{-1}$Mpc.

A much simpler dependence characterizes the outflow velocity as a function of distance for different void sizes, as can be seen in figure 6. In this figure, the left- and right-hand panels show results in real- and redshift-space respectively; upper panels show results from the galaxy distribution, lower panels from the H11.5 distribution. The different line types in these plots correspond to different void radii.

Table 2. Best fit parameter values for the maximum outflow around voids, as a function of void radius. We present the best fit parameters for voids selected from the distribution of mass, haloes and galaxies, in real-space.

Gx./halo,mass	$v_0 \mathrm{km}^{-1}\mathrm{sh}^{-1}\mathrm{Mpc}$
Mass	-22.1
H11	-16.2
H11.5	-14.5
H12	-13.2
Gx.	-14.5

In general, it can be seen that larger voids reach a minimum in velocity (or a maximum outflow) at larger separations. The outflow is also stronger for larger voids. At larger distances from void centres, velocities tend to $v = 0$ as expected given the lack of correlation of structure at these scales. Still, it should be noted that the outflow signal continues to be present at distances larger than the void size.

Figure 6 also shows that smaller voids ($r_{\rm void} < 10\mathrm{h}^{-1}\mathrm{Mpc}$) show a rapid transition in the very nearby regions, going from outflow to infall motions, revealing that these may be immersed in the middle of high density regions responsible for the infalls. Note however, that the amplitude of such infall motions is small compared to the infall motions around groups of galaxies (C05). Another contribution to this infall could originate in outflows from neighbouring voids.

We can also find out about the differences arising from identifying voids in the distribution of galaxies and dark-matter haloes in figure 6. In this visualization, the galaxy-defined voids also tend to show slightly stronger outflows than the H11.5-defined voids, and small galaxy-defined voids show a smaller degree of infall than their H11.5 counterparts. The effects of redshift-space selection simply tend to decrease the range of velocities measured around voids, that is, infall and outflow extremes are lower in absolute value, both for galaxy and H11.5-defined voids. These effects must be taken into account when comparying observational data on the dynamics of galaxies around voids with the corresponding theoretical predictions.

Figure 7 shows the dependence of the maximum outflow velocity with void radius. As can be seen, the dependence is well approximated by a linear relation with the void radius. The best fit parameters of the relation

$$v_{\rm min} = v_0 r_{\rm void} \tag{3}$$

can be found in table 2 for the different choices shown in the figure. It can be seen that mass-defined voids show a much lower and steeper maximum velocity relation when compared to galaxies, which show a difference of $\simeq 150\mathrm{kms}^{-1}$ at $r_{\rm void} \simeq 10/\mathrm{h}^{-1}\mathrm{Mpc}$ with respect to the results from mass-defined voids. In this case, it is not possible to decide which sample of halo-defined voids provides the closest outflow velocities to the galaxies, since the data from each halo sample are consistent with the galaxy-void data (which shows considerable scatter around the best fit line). Still, the results from H11.5-defined voids are characterised by the same best fit $v_0 = -14.5\mathrm{kms}^{-1}\mathrm{hMpc}^{-1}$ than the galaxy-void data.

We have also investigated the effect of using redshift-space positioning and found that the linear relation between $v_{\rm min}$ and void radius steepens considerably $\Delta v_0 < -5\mathrm{kms}^{-1}\mathrm{hMpc}^{-1}$, independently of the sample of voids used.

Finally, we also studied the possible differences in the velocity field in the directions parallel and perpendicular to the void walls. In order to do this we calculated the 1-D velocity dispersion of galaxies in both directions ($\sigma_{parallel}$ and σ_{perp}, respectively), removing the local outflow velocity when calculating the radial velocity dispersion. Our find-

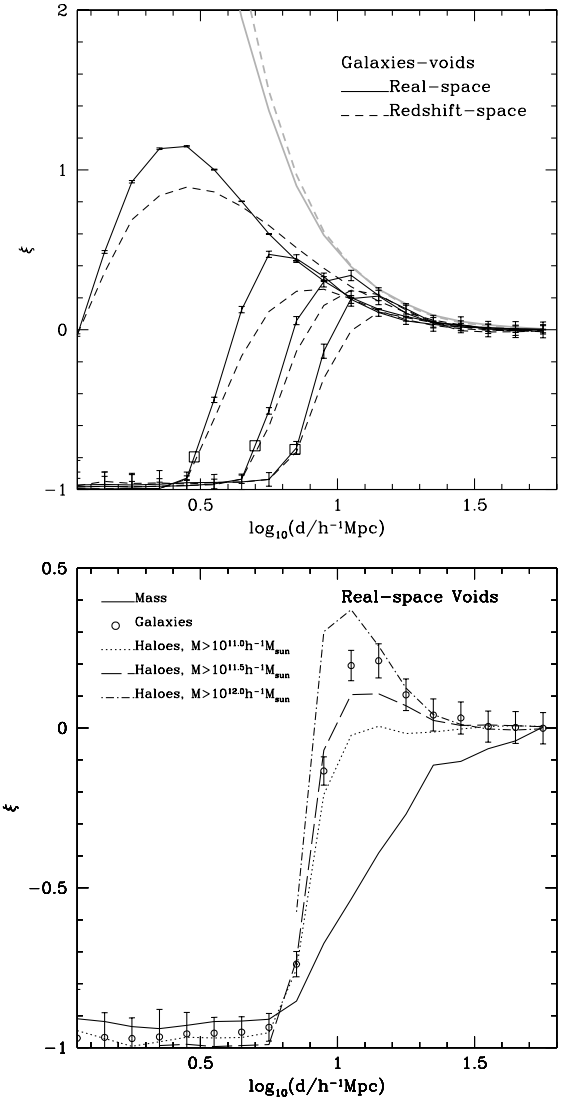

Figure 9. Upper panel: Real- and redshift-space cross correlation functions (solid and dashed lines respectively) between centres of galaxy-defined voids identified in real- and redshift-space respectively, and galaxies in the simulation. From left to right, the black solid and dashed lines represent the results for $0 < r_{\rm void}/\mathrm{h}^{-1}\mathrm{Mpc} < 2$, $2 < r_{\rm void}/\mathrm{h}^{-1}\mathrm{Mpc} < 4$, $4 < r_{\rm void}/\mathrm{h}^{-1}\mathrm{Mpc} < 6$, and $6 < r_{\rm void}/\mathrm{h}^{-1}\mathrm{Mpc} < 8$. The squares show the correlation function level at $d = r_{\rm void}$. Grey curves show the galaxy auto-correlation functions in real- (solid) and redshift-space (dashed lines). Lower panel: comparison between cross-correlations around mass-, H11-, H11.5-, H12-, and galaxy-defined voids (solid, dotted, long-dashed, dot-dashed lines and circles with errorbars, respectively) for $8 < r_{\rm void}/\mathrm{h}^{-1}\mathrm{Mpc} < 12$, in real-space.

ings are summarised in the upper panel of figure 8, where the black lines show $\sigma_{parallel}$ and the gray lines show σ_{perp}. Different line types correspond to different void radii as indicated in the key, and we only show results for voids identified using galaxies in redshift-space since there is little variation when using haloes or real-space positions. As can be seen, the velocities aligned with the radial direction from the void centre are about $10-20\%$ lower than the velocities on the direction of the void walls, regardless of void size and distance to void centre, indicating that galaxies have a slight but systematic ($2-$ to $3-\sigma$ level) tendency to follow trajectories along the void surfaces. The inset in the upper panel shows the dependence of the velocity dispersions in the directions parallel and perpendicular to the line of sight as a function of the distance to the void centre normalised by the void radius. As can be seen, at $d/r_{\rm void} \simeq 2$, the curves corresponding to different void radii converge. On the other hand, smaller voids show much higher velocity dispersions at $d/r_{\rm void} < 2$ when compared to larger voids. This is in agreement with the indication that small voids are embedded in higher density regions, which could be respondible for the high velocity dispersions in the small voids inner regions. The lower panel of this figure shows the ratio between the velocity dispersions in the directions parallel and perpendicular to the void walls, and as can be seen there is little dependence on the distance to the void centre and on the void radius, being consistent with a roughly constant $\sigma_{parallel}/\sigma_{perp} = 1.1$.

The observational study of the peculiar velocity field around voids is carried out in a forthcoming paper, Ceccarelli et al. (2004), where the different observational biases present in peculiar velocity data are analysed, and the results are compared to the theoretical expectations presented here.

4 CORRELATIONS AROUND VOIDS

We now focus our attention on the spatial statistics of galaxies, haloes and mass around voids. We use the 2-point cross correlation function between void centres, and galaxies, haloes or dark-matter particles to characterise the spatial clustering properties of the vicinities of voids. In the following subsections we study the 1-dimensional cross-correlation function in real- and redshift-space, and the cross-correlation function as a function of the coordinates perpendicular and parallel to the line of sight.

4.1 1-Dimensional correlation functions

In this subsection we study the spatial correlations between the void centres and the objects surrounding them. We will compare once more the resulting statistics from considering voids in the distribution of galaxies, haloes and mass, using real- and redshift-space positions.

We start by analysing our expectations for the outcome of a void-object cross-correlation function, which we compute using the following estimator,

$$\xi(r) = \frac{d_c d_o}{d_c r_o} - 1, \qquad (4)$$

where $d_c d_o$ corresponds to the number of center-object pairs, and $d_c r_o$ is the number of center-random pairs which would be measured if the positions of objects were uniformly distributed in space. The latter is calculated using the mean density of objects in the numerical simulation box. What we expect to find at small separations is an anti-correlation, lower in amplitude than the maximum overdensity set for identifying voids, that is, $\xi < -0.9$. On the other hand, at sufficiently large separations, $d \simeq r_{\rm void}$, we would expect to find departures from this value and to gradually tend towards a small but positive value for the correlation function, indicating a population of galaxies at the void walls. We also expect $\xi \simeq 0$ at sufficiently large separations from the void centres.

Figure 9 shows the cross-correlation functions between galaxy-defined voids and galaxies (upper panel), and galaxy-, halo- and mass-defined voids with their respective counterparts, in real space (lower panel). Solid and dashed lines in the upper panel represent the results in real- and redshift-space respectively. Concentrating on the results for galaxy-defined voids, it can be seen that we obtain the expected value $\xi < -0.9$ at low separations for void radii $r_{\rm void} > 4{\rm h}^{-1}$Mpc in real- and redshift-space (Smaller voids may show this effect at lower separations than those analysed in this work), and also that at the void radius, $\xi(r_{\rm void}) \simeq -0.9$ (open squares). This relation holds regardless of the tracer used to identify voids. The general effect produced by changing from real- to redshift-space data, where the voids are identified in redshift-space and the tracers are also in redshift-space, is that of lowering very slightly the maximum clustering amplitude.

Another important feature of the correlation functions shown in the upper panel of figure 9 is that at separations, $d \simeq r_{\rm void}$, ξ increases rapidly in value reaching $xi > 0$, but always lower than the galaxy auto-correlation function. It is also noticeable the fact that the correlation function around voids can be positive outside the void radius, particularly for the smaller voids, $r_{\rm void} < 4{\rm h}^{-1}$Mpc, which can be interpreted as small voids being embedded in extended, reasonably high density regions, in accordance with the results from the velocity field around small voids, which shows systematic infalls instead of outflows. Note that this peak in ξ is still quite low compared to the galaxy correlation function.

From the comparison between results for different void populations in the lower panel of figure 9, we see that mass-defined voids show a higher cross-correlation function than haloes and galaxies at $d < r_{\rm void}$. Haloes, on the other hand, show the same correlation levels than galaxies at small separations from the void centres. At larger separations, $d > r_{\rm void}$, individual dark-matter particles are less clustered than galaxies. Haloes show a range of clustering amplitudes which correlates with the halo mass. In particular, H11.5 show consistent correlation amplitudes than galaxies, and H12 show higher ξs.

It is interesting to note though, that independently of the object used to identify voids, the cross-correlation function shows a similar qualitative shape, starting off at a constant negative value at low separations, independent of void radius, and increasing at separations of the order of the void radii, approaching $\xi = 0$. Note that this change from negative to $\xi \simeq 0$ is sharper for haloes and galaxies than for mass-defined voids. For instance, for $r_{\rm void} > 8{\rm h}^{-1}$Mpc, the

galaxy-void - galaxy cross-correlation function values are as high as the galaxy ξ.

Given the clear correlation between the void-size and the distance at which the correlation amplitude departs from its constant negative value, we have also calculated the density profiles around voids as a function of the reduced distance to the void centres, $d/r_{\rm void}$ (figure 10). As can be seen, density profiles for voids with $r_{\rm void} > 8{\rm h}^{-1}$Mpc are marginally consistent with one another ($2-\sigma$).

The comparison between the density profiles of different void populations, shown in the middle panel of figure 10, is similar to what was found for cross-correlation functions. Namely, we find that the density profiles of mass-defined voids are lower in amplitude than galaxy-defined voids. The latter are found to be of similar amplitudes than the density profiles of halo-defined voids, in agreement with the numerical simulation results by Gotlöber et al. 2003. On large separations $d/r_{\rm void} > 1$, small voids with $r_{\rm void} < 8{\rm h}^{-1}$Mpc show density profiles much higher than larger voids with $r_{\rm void} > 8{\rm h}^{-1}$Mpc.

The differences in $\rho/ < \rho >$ for the different types of void can be alleviated significantly by dividing the density profile by the correlation function of the objects used to identify the voids (see the lower panel of figure 10). In this case, the density profiles divided by the correlation function of galaxies are in better agreement with one another for a wider range of void sizes, $r_{\rm void} > 2{\rm h}^{-1}$Mpc. In addition, this ratii can be fitted by the empirical function,

$$\frac{\rho(r)}{<\rho>(1+\xi)} = 1 - A_1 \exp\left[-\left(A_2\frac{d}{r_{\rm void}}\right)^c\right]. \qquad (5)$$

The parameter A_1 is related to the density contrast threshold used for defining the voids ($\delta = -0.9$ in our case), and to whether galaxies, haloes or mass are used as the tracers of the density field. A_2 depends strongly on the tracer and on the maximum density contrast used to identify the voids. The parameter c indicates how rapid is the change from constant negative density contrast to the mean density of the Universe and also depends strongly on the tracer. Table 3 summarises the parameter values corresponding to the different choices we show in the figure. The use of different void-finding algorithms will also change the values of the quoted best-fit parameters. For instance, the use of the distance to the closest object (as in Gotlöber et al. 2003), will lower the value of A_2 to compensate for the typically smaller radii found by this void-finding method.

The thick dot-dashed line in the inset shows again the fit in the main panel, this time divided by the galaxy correlation function; the χ^2 per degree of freedom is always lower than 1 for $r_{\rm void} > 4{\rm h}^{-1}$Mpc in this case. As a final check, we have corroborated that this level of coincidence between density profiles divided by correlation functions also holds for H11-, H11.5-, H12-, and mass voids.

In sum, we find that voids with $r_{\rm void} > 8{\rm h}^{-1}$Mpc, show a nearly universal radial profile for the ratio involving the density profile of objects and the 2-point auto-correlation function, $\rho/(<\rho>(1+\xi))$. This is true for voids identified from both, galaxies and dark-matter haloes. The best fit parameters for the density profiles are presented in table 3. Since voids of any size (within the limits imposed by the numerical simulation available for this work, $2 < r_{\rm void}/{\rm h}^{-1}{\rm Mpc} < 30$) show similar radial $\rho/(<\rho>(1+\xi))$

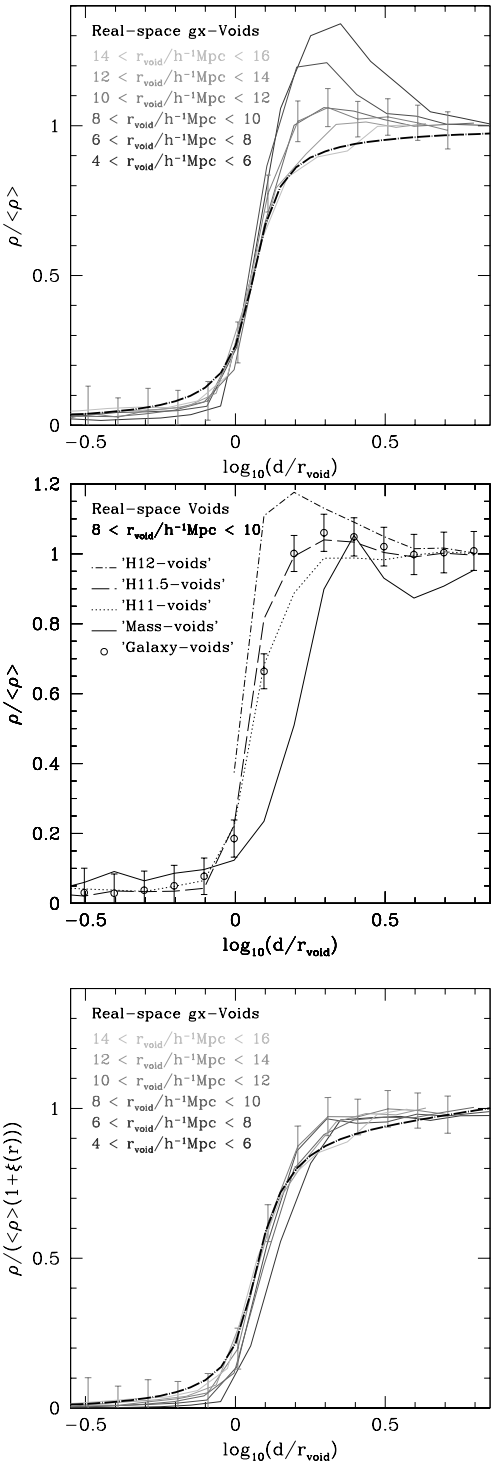

Figure 10. Upper panel: Real-space density profiles around centres of galaxy-defined voids (circles and triangles respectively) in the simulation as a function of reduced distance, $d/r_{\rm void}$. Gray-scale lines represent the results for $8 < r_{\rm void}/{\rm h}^{-1}{\rm Mpc} < 10$, $10 < r_{\rm void}/{\rm h}^{-1}{\rm Mpc} < 12$, $12 < r_{\rm void}/{\rm h}^{-1}{\rm Mpc} < 14$, and $14 < r_{\rm void}/{\rm h}^{-1}{\rm Mpc} < 16$ (lighter to darker gray-scale). The dot-dashed line shows the the empirical fit (see text) for the galaxy-void density profile. Lower panel: comparison between the measured density profiles of mass-, H11-, H11.5-, H12-, and galaxy-defined voids (solid, dotted, long-dashed, dot-dashed lines and circles with errorbars, respectively) for $8 < r_{\rm void}/{\rm h}^{-1}{\rm Mpc} < 12$, in real-space.

Table 3. Best fit parameters, A_1, A_2 and c, for the density profile of dark-matter particles, dark-matter haloes and galaxies, around mass- halo- and galaxy-defined voids respectively, $\rho(r)/ < \rho >= 1 - A_1 \exp\left[-\left(A_2 \frac{d}{r_{\rm void}}\right)^c\right]$.

Real/Redshift-space	Gx./mass	A_1	A_2	c
Real	Mass	0.90	0.60	5.0
	H11	0.96	0.80	5.5
	H11.5	0.97	0.85	7.0
	H12	0.98	0.89	8.0
	Gx.	0.96	0.80	6.0
Redshift	Mass	0.90	0.65	5.0
	H11	0.95	0.85	5.5
	H11.5	0.96	0.90	6.0
	H12	0.98	0.93	7.0
	Gx.	0.95	0.80	5.0

profiles. The parameters in the table also describe this profile provided the fit is divided by the correlation function of the tracers used when constructing the sample of voids.

4.2 Redshift-space distortions

We study the galaxy-void - galaxy and halo-void - halo cross-correlation functions, $\xi(\sigma,\pi)$, as a function of the coordinates parallel (σ) and perpendicular (π) to the line of sight, which we take to be the $z-$axis of the numerical simulation. In order to simulate the redshift-space distortions we again displace the positions of dark-matter haloes and galaxies by the projection onto the z-axis of their peculiar velocities and measure $\xi(\sigma,\pi)$. In order to visualize this 2-dimensional distorted function, we study the the contours of constant correlation amplitude in the $\sigma-\pi$ plane. We remind the reader that the iso-correlation contours for a $\xi(\sigma,\pi)$ measured using real-space positions would correspond to circles, since there are no preferred directions in the simulation and the correlation function must therefore be isotropic. However, as we use redshift-space positions, we can learn about the dynamical properties of galaxies, dark-matter haloes and individual particles around voids from the departure of contour shapes from perfect circles. Such departures are commonly known as redshift-space distortions.

Redshift-space distortions have been extensively studied for all kinds of objects, including quasars (Hoyle et al. 2002), galaxies (Loveday et al. 1995, Rattclife et al. 1998), groups (Padilla et al. 2001), and clusters of galaxies (Bahcall & Cen 1992, Padilla & Lambas 2003a and 2003b). Also, assuming that redshift-space distortions around voids are not important, Ryden (1995) proposed using the cosmological distortions around voids for measuring q_0.

At small separations, the galaxy correlation function, $\xi(\sigma,\pi)$, shows elongations in the direction of the line of sight due to their random motions in the interiors of clusters of galaxies (Loveday et al. 1995). At larger separations, it is possible to see infall motions toward large mass concentrations (Hawkins et al. 2003). The effect of infall motions was first measured using galaxy groups in the UZC by Padilla et al. (2001). The advantage of using groups relies in the fact that they only show infall signatures in their distortion patterns, which induces a flattening of the correlation function contours in the direction of the line of sight.

Voids are the opposite of galaxy groups in terms of their surrounding peculiar velocity field, so we expect to find an elongation of the correlation function contours along the line of sight. This is expected to affect not only small separations in the σ direction, as is the case with the fingers of god signatures in the galaxy $\xi(\sigma,\pi)$, but also larger σ separations. Figure 11 shows the correlation function contours corresponding to H11.5- and galaxy-defined voids (left- and right-hand panels respectively) as a function of normalised separation in the directions parallel and perpendicular to the line of sight (in our case, the line of sight coincides with the z-axis in the simulation box). The void radius increases from bottom to top panels, with values in the ranges shown in the key on each panel. The different line types represent different correlation function amplitudes; solid lines correspond to $\xi \leq 0$ and dotted lines to $\xi > 0$. In order to facilitate the interpretation of this figure, and the comparison to results from the auto-correlation function of galaxies, the reader is referred to figure 4 in Hawkins et al. (2003), which shows estimates of $\xi(\sigma,\pi)$ for different galaxy types in the 2dFGRS.

As expected, the void-halo cross-correlations show elongated iso-correlation contours along the line of sight, specially for the $\xi < 0.0$ contours. This can also be found in the void-galaxy cross correlations, in particular for the lower correlation function contours, $\xi < -0.3$. Also, as can be seen in the figure, the contour patterns contain an unexpected wealth of information which we analyse in detail in what follows.

(i) The iso-ξ contours around voids differ from the elongations seen in galaxy auto-correlation functions since here the elongated patterns extend out to separations $\sigma \simeq r_{void}$, perpendicular to the line of sight (ranging from 4 to 14h^{-1}Mpc from bottom to top panels). On the other hand, the galaxy auto-correlation function is significantly distorted only out to $\sigma \simeq 2$h^{-1}Mpc (Hawkins et al. 2003).
(ii) As expected, Galaxy- and H11.5-void $\xi(\sigma,\pi)$ show a positive correlation signal in agreement with the results from the 1-dimensional correlation functions from the previous section. The patterns corresponding to positive correlations show the finger-of-god effect taking place at the void boundaries.

- (iii) The flattening of the patterns beyond this radius is originated in random motions taking place in the void walls, which correspond to a radial velocity dispersion $\sigma_{perp} \simeq 300$kms^{-1} (see figure 8).

(iv) There are usually two $\xi = 0$ contours in the void $\xi(\sigma,\pi)$ diagrams. The first one (closer to the origin) corresponds to the increase in density at the void walls. The second $\xi = 0$ contour (further away from the origin) is determined by the end of large scale fluctuations.
(v) H11.5 haloes show an outflow motion of lower amplitude than that of galaxies. However, since halos have a larger velocity dispersion in the void edges, they appear with a smaller radial elongation than galaxies.

The elongations along the line of sight seen in the 2-dimensional correlation function of voids can be used to infer the peculiar velocity field around voids without the need of measuring peculiar velocities. The latter is a difficult

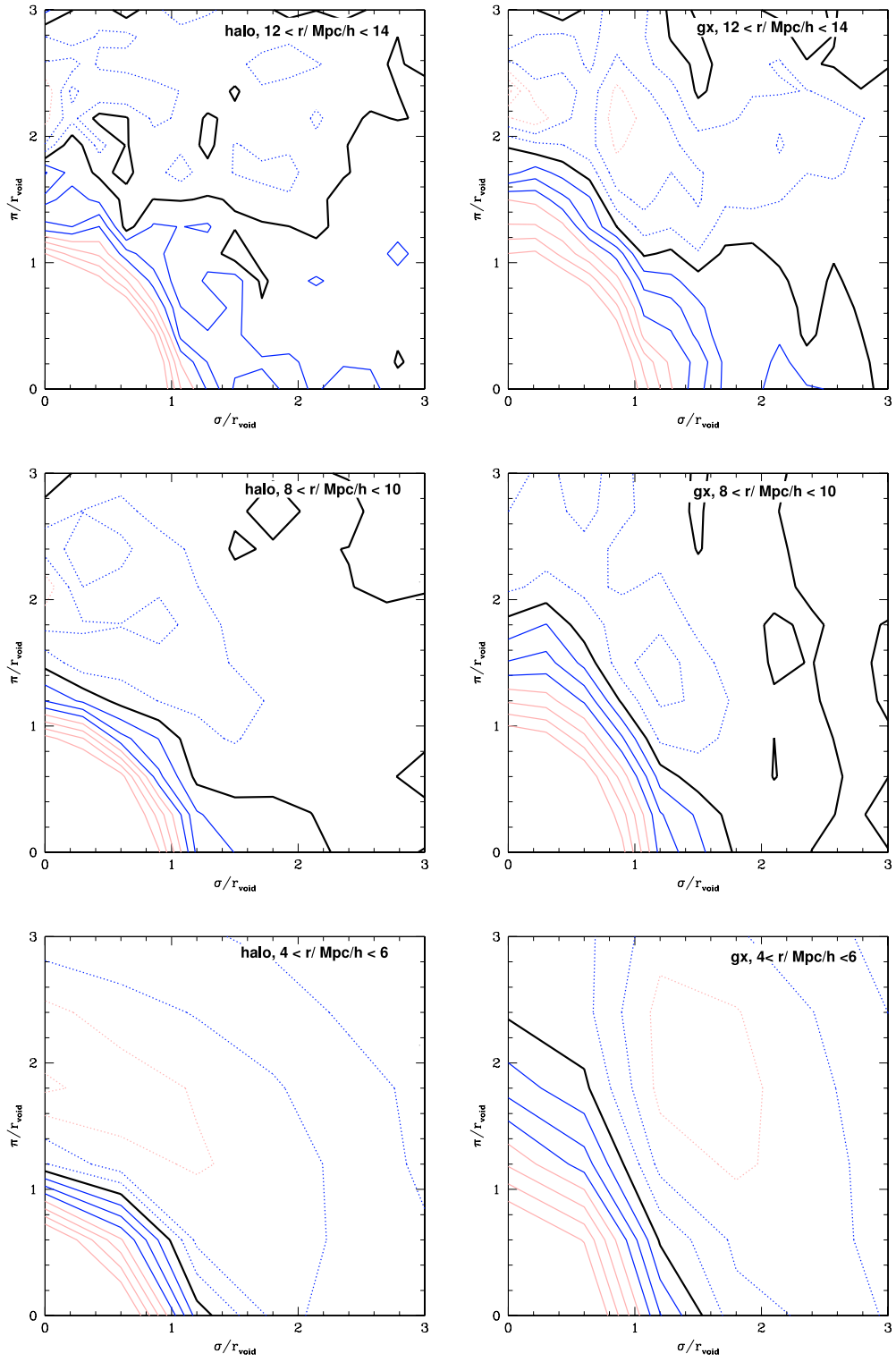

Figure 11. Redshift-space void-halo (left) and void-galaxy (right) cross correlation functions as a function of the normalised coordinates parallel (π/r_{void}) and perpendicular (σ/r_{void}) to the line of sight (the z-axis in the numerical simulation). Here the centres of voids are those identified in redshift-space. The solid red (gray) lines represent $\xi(\sigma,\pi) = -0.6, -0.5, -0.4$, solid blue (black) lines $\xi(\sigma,\pi) = -0.3, -0.2, -0.1$, the thick solid line corresponds to $\xi(\sigma,\pi) = 0.0$. The dotted blue (black) lines show $\xi(\sigma,\pi) = 0.1, 0.2$, and the red (gray) dotted lines, $\xi(\sigma,\pi) = 0.3, 0.4$, and 0.5.

Table 4. Summary of main differences in the statistics related to voids, when using galaxies and dark-matter (particles or haloes), in real- and redshift-space.

Statistic	Real or Redshift-space	Gx., haloes and mass
Number density	Redshift space is higher by up to factor 2.5 at large void radius. Consistent at $r_{\rm void} < 4{\rm h}^{-1}$Mpc for mass-voids. Halo- and galaxy-defined voids show smaller changes from real- to redshift-space.	The number density of Galaxy-defined voids is higher than that of mass-defined voids by as much as two orders of magnitude: consistent at $r_{\rm void} < 4{\rm h}^{-1}$Mpc, but no mass-haloes at $r_{\rm void} > 12{\rm h}^{-1}$Mpc. H11.5- and H12 haloes in agreement with galaxy-defined voids.
Void ξ		Galaxy-defined voids show stronger auto-correlation functions than halo-void ξs. Shape of void ξ for voids with different radii are similar, and amplitude increases with $r_{\rm void}$.
Outflow velocity	Slower outflows and infalls in redshift-space (by about $30{\rm kms}^{-1}$.	Galaxy-defined voids show similar infall and outflow motions to H11.5-defined voids (differences $< 20{\rm kms}^{-1}$)
1D ξ	Increase in ξ at $r = r_{void}$ is milder when voids and tracers are in redshift-space.	Galaxy ξ is quite higher than mass ξ outside the void radius. Inside the void radius both ξs are almost indistinguishable. Good agreement between galaxy- and H11-defined voids.
2D ξ	Real-space shows no anisotropies as expected. Redshift-space elongations extending out to $\sigma \propto r_{\rm void}$.	Galaxy-defined voids show larger elongations in $\xi(\sigma, \pi)$ than H11.5-defined voids. Qualitatively, the shapes of contours are similar for both types of voids.

task due to the large errors involved in the measurement of distances by means independent of redshift. We tackle this problem in a forthcoming paper, Ceccarelli et al. (2005a).

5 SUMMARY AND CONCLUSIONS

In this work we studied the statistical properties of voids selected from the distribution of mass, haloes and $B_J < -16$ galaxies in a ΛCDM numerical simulation populated with galaxies using a GALFORM semi-analytic galaxy formation model (Cole et al. 2000). The aim of this work was to understand the systematic biases between these different void populations (Patiri et al. 2004, Gottlöber et al. 2003).

We find that the number density of galaxy-defined voids departs from that of mass-defined voids at $r_{\rm void} \geq 4{\rm h}^{-1}$Mpc. However, the fraction of the volume of the simulation box in galaxy-defined voids and voids identified from haloes with $M > 10^{11.5}{\rm h}^1$ $M_\odot$ (H11.5-defined voids) are compatible with one another. The effect of identifying voids in redshift space increases the number of voids in the simulation, but this effect is almost negligible for galaxy- and halo-defined voids. The fraction of total volume occupied by galaxy voids in the simulation reaches the 30% level when considering voids with $r_{\rm void} > 3{\rm h}^{-1}$Mpc. This fraction is considerably smaller than results obtained from redshift surveys by Hoyle & Vogeley (2002), who find that about 50% of the volume in the Universe is in larger voids. In order to properly assess whether this disagreement is significant, it must be taken into account that the volume fraction in voids is very sensitive to the abundance of large voids in the sample analysed. Therefore, it would be necessary to analyse larger simulations than the one used in this work to be able to make a more reliable comparison. Another factor that influences the volume fraction in voids is the density contrast used to identify voids; a higher density contrast increases slightly the fraction of volume. In addition, the identification of voids in redshift space also produces this effect, bringing the results from our simulation even closer to observational estimates.

The study of the auto-correlation function of voids shows that voids identified from more massive haloes show a higher auto-correlation function. In particular, H12-defined voids show a correlation function which is in agreement with that of galaxy-defined voids. Still, the clustering of voids is very weak, with amplitudes almost always lower than $\xi = 1$. We found that the shape of the auto-correlation function of voids is consistent with being independent of void radius. The amplitude, however, is seen to increase with void size. By using 100 sets of random catalogues of voids which satisfy the same exclusion constraints as galaxy- and halo-defined voids, we demonstrate that the void auto-correlation function can not be associated solely to an artifact of the void identification procedure. The average random-voids correlation function shows a similar shape than that of galaxy-defined voids, but also shows a lower amplitude indicating a

possible influence from hierarchical clustering on the galaxy-defined void auto-correlations.

The study of the outflow velocities around voids shows outflow velocities which reach a maximum at a distance, $d_{\rm vmin} \sim r_{\rm void}$. At larger separations, $d_{\rm zero}$, the outflow velocities become moderate infall motions due to the higher density of the void walls and outflow motions from neighbouring voids. We find that a very simple relation that describes $d_{\rm vmin}$ and $d_{\rm zero}$ as a function of void radius, with parameters that can be found in table 1. Table 2 shows the linear fit parameters for the relation between void radius and maximum outflow motions, $r_{\rm void}$ vs. $v_{\rm min}$. We searched for differences in the velocity field of galaxies and dark-matter haloes around voids, and found that galaxy-defined voids show similar outflows to H11.5-defined voids. Also, the use of redshift space data lowers the extreme values of velocities around voids, that is, both outflows and infalls appear less important than in real-space. We also analysed the galaxy velocity dispersion at the void walls, and find a systematically larger velocity dispersion in the direction parallel to the void walls with respect to the radial direction (a $\simeq 10-20\%$ difference).

We find that the cross-correlation functions between voids and galaxies, haloes and mass show negative constant values out to separations comparable with the void size. At larger separations the galaxy-void - galaxy correlation function level increases to approach the auto-correlation function of the galaxies. The amplitude of the correlation function of galaxies near the centres of galaxy-defined voids is slightly lower than that of the mass around mass-defined voids.

We also studied the distortion pattern observed in $\xi(\sigma,\pi)$ and found an elongation along the line of sight. This elongation differs from that found in the galaxy auto-correlation function, as this effect extends out to large separations perpendicular to the line of sight. The study of these elongations would allow us to obtain properties of the velocity field around voids using only measured redshifts, which are much easier to obtain observationally than galaxy peculiar velocities. The study of $\xi(\sigma,\pi)$ not only provides information about the peculiar velocity field around voids, but also on finger-of-god motions at the void walls through the elongation of $\xi > 0.1$ contours along the line of sight, at separations $\pi \simeq 2-3r_{\rm void}$.

We find that the study of voids selected from the distribution of galaxies can provide biased results which can not easily be reconciled with results from dark-matter haloes. For instance, the number density of voids as a function of radius for galaxy-defined voids is in agreement with that of H12-defined voids for large void radii, and with H11.5 voids at small radii. Also, the void auto-correlation function of galaxy-defined voids is in better agreement with H12-defined voids, than with H11.5-defined voids; the velocity field of galaxies is in better agreement with H11.5-defined voids. However, the elongations in the galaxy-void $\xi(\sigma,\pi)$ are qualitatively matched by H11.5-haloes. Therefore care must be taken when making an interpretation based on galaxy-void data. We present table 4 as an overall summary of the differences between properties of voids selected from galaxies and dark-matter haloes in real- and redshift-space.

It can be argued that, observationally, the easiest way to obtain the velocity field surrounding voids is the 2-dimensional correlation function $\xi(\sigma,\pi)$. We analyse whether it is possible to estimate directly the peculiar velocity field around voids from peculiar velocity data, and also measure $\xi(\sigma,\pi)$ using large observational datasets such as 2dFGRS and SDSS in the next step of this work, which at present is being carried out in a forthcoming paper (Ceccarelli et al., 2005a), where we pay special attention to many observational biases such as distance measurement errors, irregular angular completeness masks and flux limit effects.

ACKNOWLEDGMENTS

This work was supported in part by the ESO-Chile Joint Committee, NDP was supported by a Proyecto Postdoctoral Fondecyt no. 3040038. DGL and LC are supported by CONICET. We thank the Durham group for providing the semi-analytic galaxy formation and simulation dark-matter outputs used in this work. We thank the Referee for helpful comments and suggestions.

REFERENCES

Bahcall, N.A., & Cen, R. 1992, ApJ, 398, 81.
Ceccarelli, L., et al., 2005a, in preparation (C05).
Ceccarelli, L., Valotto, C.A., Lambas, D.G., Padilla, N.D., Giovanelli, R., & Haynes, M., 2005b, accepted for publication in ApJ.
Cole, S., Lacey, C.G., Baugh, C.M., & Frenk, C.S., 2000, MNRAS, 319, 168.
Croton, D.J., et al. (the 2dFGRS Team), 2004, submitted to MNRAS, astro-ph/0401406.
Einasto, J., Einasto, M., & Gramman, M., 1989, MNRAS, 238, 155.
El-Ad H., & Piran, T., 1997, ApJ, 491, 421.
El-Ad H., & Piran, T., 2000, MNRAS, 313, 553.
Geller, M.J., & Huchra, J.P., 1989, Sci, 246, 897.
Ghigna, S., Bonometto, S.A., Retzlaff, J., Gottloeber, S., & Murante, G., 1996, ApJ, 469, 40.
Goldberg, D.M., Jones, T.D., Hoyle, F., Rojas, R.R., Vogeley, M.S., & Blanton, M.R., 2004, submitted to ApJ, astro-ph/0406527.
Gottlöber S., Lokas, E.L., Klypin, A., & Hoffman, Y., 2003, MNRAS, 344, 715.
Gregory S.A., Thompson, L.A., 1978, ApJ, 222, 784.
Hawkins, E., et al. (the 2dFGRS Team), 2003, MNRAS, 346, 78.
Hoffman, Y., & Shaham, J., 1982, ApJ, 262, L23.
Hoyle, F., Outram, P.J., Shanks, T., Boyle, B.J., Croom, S.M., & Smith, R.J., 2002, MNRAS, 332, 311.
Hoyle, F., & Vogeley, M.S., 2002, ApJ, 566, 641.
Hoyle, F., Rojas, R.R., Vogeley, M.S., & Brinkmann, J., 2003, submitted to ApJ, astro-ph/0309728.
Joeveer, M., Einasto, J., Tago, E., 1978, MNRAS, 185, 357.
Kirshner, R. P., Oemler, A., Schechter, P. L., Shectman, S. A., 1981, ApJ, 248, 57.
Loveday, J., Maddox, S.J., Efstathiou, G., & Peterson, B.A., 1995, ApJ, 442, 457.
Müller, V., Arbabi-Bidgoli, S., Einasto, J., & Tucker, D., 2000, MNRAS, 318, 280.
Padilla, N.D., Merchán, M., Valotto, C., Lambas, D.G., & Maia, M., 2001, ApJ.
Padilla, N.D. & Baugh, C.M., 2003, 343, 796.
Padilla, N.D. & Lambas, D.G., 2003a, MNRAS, 342, 532.
Padilla, N.D. & Lambas, D.G., 2003b, MNRAS, 342, 519.
Patiri, S.G., Betancort-Rijo, J.E., & Prada, F., 2004, submitted to ApJ, astro-ph/0407513.

Peebles, P.J.E., 1982, ApJ, 257, 438.
Peebles, P.J.E., 2001, ApJ, 557, 495.
Percival, W., et al. (the 2dFGRS Team), 2004, MNRAS Accepted, astro-ph/0406513.
Plionis, M., & Basilakos, S., 2002, MNRAS, 330, 399.
Ryden, B.S., 1995, ApJ, 452, 25.
Spergel, D.N., et al. (the WMAP team), 2003, ApJS, 148, 175.
van de Weygaert, R., Sheth, R., & Platen, E., 2004, Proceedings IAU Colloquium, 195.
Vogeley, M.S., Geller, M.J., Park, C., & Huchra, J.P., 1994, AJ, 108, 745.
White, S. D. M., 1979, MNRAS, 186, 145.